inorganics

MDPI

Communication

Halogen Substituent Effect on the Spin-Transition Temperature in Spin-Crossover Fe(III) Compounds Bearing Salicylaldehyde 2-Pyridyl Hydrazone-Type Ligands and Dicarboxylic Acids

Takumi Nakanishi [1], Atsushi Okazawa [2] and Osamu Sato [1,*]

[1] Institute for Materials Chemistry and Engineering, Kyushu University, 744 Motoka, Nishi-ku, Fukuoka 819-0395, Japan; nakanishi.takumi.316@m.kyushu-u.ac.jp

[2] Department of Basic Science, Graduation School of Arts and Sciences, The University of Tokyo, 3-8-1 Komaba, Meguro-ku, Tokyo 153-8902, Japan; cokazawa@mail.ecc.u-tokyo.ac.jp

* Correspondence: sato@cm.kyushu-u.ac.jp; Tel.: +81-92-802-6208; Fax: +81-92-802-6205

Received: 29 June 2017; Accepted: 11 August 2017; Published: 12 August 2017

Abstract: Four Fe(III) spin-crossover (SCO) compounds, $[Fe(HL1)_2](HCl_4TPA)$ (**1-Cl**), $[Fe(HL1)_2](HBr_4TPA)$ (**1-Br**), $[Fe(HL2)_2](HCl_4TPA)$ (**2-Cl**), and $[Fe(HL2)_2](HBr_4TPA)$ (**2-Br**) (HL1 = 4-chloro-2-nitro-6-(1-(2-(pyridine-2-yl)hydrazono)ethyl)phenolate; HL2 = 4-bromo-2-nitro-6-(1-(2-(pyridine-2-yl)hydrazono)ethyl)phenolate; HCl_4TPA = 2,3,5,6-tetrachloro-4-carboxybenzoate; and HBr_4TPA = 2,3,5,6-tetrabromo-4-carboxybenzoate), were synthesized to investigate the halogen substituent change effect in salicylaldehyde 2-pyridyl hydrazone-type ligands and dicarboxylic acids in SCO complexes to the spin-transition temperature. Crystal structure analyses showed that these compounds were isostructural. In addition, a one-dimensional hydrogen–bonded column was formed by the dicarboxylic acid anion and weak hydrogen bonds between the Fe(III) complexes. From Mössbauer spectroscopy and magnetic property measurements, these compounds were confirmed to exhibit gradual SCO. The spin-transition temperature can be shifted by changing the halogen substituent in the salicylaldehyde 2-pyridyl hydrazone-type ligands and dicarboxylic acids without changing the molecular arrangement in the crystal packing.

Keywords: spin crossover; hydrazone complex; dicarboxylic acid

1. Introduction

Spin-crossover (SCO) complexes have attracted considerable attention as materials for developing memory devices because the spin state can be switched by external stimuli such as temperature, light, and pressure [1–3]. In terms of practical applications, it is preferable for the spin-transition temperature to be near room temperature. Therefore, the effects of replacing anion and solvent molecules and the introduction of substituents into ligands on the spin-transition temperature have been actively studied for many types of SCO complexes [4–16].

As an approach toward shifting the spin-transition temperature, we focused on the effect of halogen substituent changes in the ligands and coexisting molecules, particularly in a carboxylic acid. In our previous study, we developed an Fe(II) SCO compound containing a neutral Fe(II) complex and a halogen-substituted dicarboxylic acid [17]. The halogen substituent change on the dicarboxylic acid molecule was confirmed to affect the spin-transition temperature while maintaining the molecular arrangement of the complex. Fe(III) SCO complexes have a great advantage over Fe(II) SCO complexes in terms of in-air stability; thus, Fe(III) SCO complexes have attracted considerable attention and have been actively developed [18–24]. In this study, we aim to introduce a halogen-substituted dicarboxylic acid into Fe(III) SCO compounds as an anion and confirm the effect of the halogen

substituent change in the dicarboxylic acid to the spin-transition temperature. Simultaneously, the effect of the halogen substituent change in the ligand to the spin-transition temperature was also investigated. Salicylaldehyde 2-pyridyl hydrazone-type ligands can form 1+ cationic Fe(III) complexes [25–28]. Those that bear 2-methoxy-6-(pyridine-2-ylhydrazonomethyl)phenol exhibit SCO properties [24]. However, there are no reports on the effect of changing the halogen substituent on the salicylaldehyde 2-pyridyl hydrazone-type ligand to the spin-transition temperature because Fe(III) SCO complexes bearing such ligands are scarcely reported. In this study, we synthesized two ligands, 4-chloro-2-nitro-6-(1-(2-(pyridine-2-ylhydrazonoethyl)phenol)) (H_2L1) and 4-bromo-2-nitro-6-(1-(2-(pyridine-2-ylhydrazonoethyl)phenol)) (H_2L2), and tetrachloroterephthalic acid (H_2Cl_4TPA) and tetrabromoterephthalic acid (H_2Br_4TPA) were used as the halogen-substituted dicarboxylic acids (Scheme 1). In total, four SCO compounds, $[Fe(HL1)_2](HCl_4TPA)$ (**1-Cl**), $[Fe(HL1)_2](HBr_4TPA)$ (**1-Br**), $[Fe(HL2)_2](HCl_4TPA)$ (**2-Cl**), and $[Fe(HL2)_2](H_2Br_4TPA)$ (**2-Br**), were obtained. The crystal structures, Mössbauer spectra, and magnetic properties of these compounds were investigated.

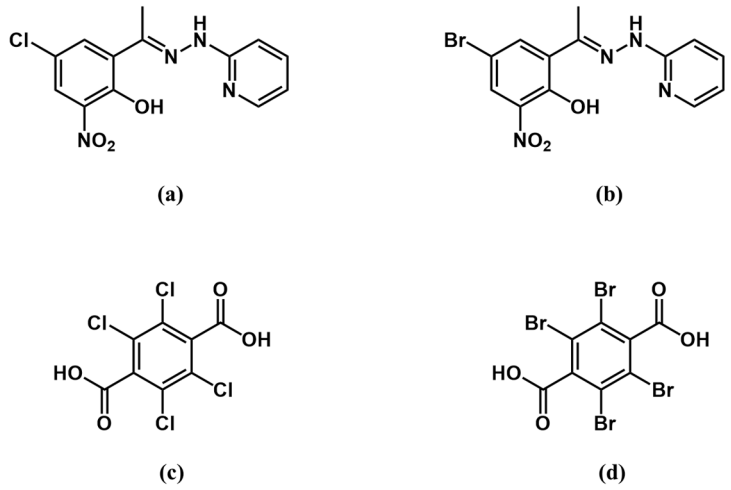

Scheme 1. Structural formula of (**a**) H_2L1; (**b**) H_2L2; (**c**) H_2Cl_4TPA; and (**d**) H_2Br_4TPA.

2. Results and Discussion

2.1. Synthesis and Characterization

The following starting materials were commercially available: 5′-chloro-2′-hydroxy-3′-nitroacetophenone, 5′-bromo-2′-hydroxy-3′-nitroacetophenone, 2-hydrazinopyridine, $FeCl_3{\cdot}6H_2O$, H_2Cl_4TPA, H_2Br_4TPA, and trimethylamine. HL1 and HL2 were obtained from the typical procedure to synthesize salicylaldehyde 2-pyridyl hydrazone-type ligands [29]. Equimolar 5′-chloro-2′-hydroxy-3′-nitroacetophenone or 5′-bromo-2′-hydroxy-3′-nitroacetophenone and hydrazinopyridine were added to ethanol, and the solution was refluxed for 5 h. Subsequently, the solution was left to stand for several days. Yellow needle-shaped crystals were obtained. **1-Cl** and **1-Br** were obtained by the reaction of H_2L1 with $FeCl_3{\cdot}6H_2O$ and H_2Cl_4TPA or H_2Br_4TPA with equal parts of trimethylamine in methanol, respectively. The synthesis procedures for **2-Cl** and **2-Br** were identical to those for **1-Cl** and **1-Br**, respectively, except that H_2L2 was used instead of H_2L1. Plate-shaped black-brown crystals were obtained. Each Fe(III) compound was characterized by elemental analysis and single-crystal X-ray measurements.

2.2. Crystal Structure

The crystal structures of **1-Cl** were determined at 123 and 330 K, and those of **1-Br**, **2-Cl**, and **2-Br** were determined at 123 K. The crystallographic data of **1-Cl**, **1-Br**, **2-Cl**, and **2-Br** are summarized in

Table 1. The coordination distances and intermolecular interactions of **1-Cl**, **1-Br**, **2-Cl**, and **2-Br** are summarized in Table 2. The asymmetric unit of **1-Cl** at 123 K shows half of the Fe(III) complex and half of the dicarboxylic acid molecule without any solvent molecules (Figure 1a). The half Fe(III) complex and the half dicarboxylic acid molecule in the asymmetric unit indicate that the two ligands in the Fe(III) complex are crystallographically identical and the two carboxyl groups in the dicarboxylic acid molecule are also crystallographically identical. The molecular arrangement of the Fe(III) complexes and the dicarboxylic acid molecules is illustrated in Figure 1b. The dicarboxylic acid molecules were confirmed to form a one-dimensional (1D) column through hydrogen bonds between each carboxyl group. Because a hydrogen bond is formed between each dicarboxylic acid molecule, it was predicted that (i) one of the two carboxyl groups in each H_2Cl_4TPA molecule was deprotonated and (ii) **1-Cl** is comprised of one HCl_4TPA^- anion and one $[Fe^{III}(HL)_2]^+$ cation. The $O^-\cdots H^+\cdots O^-$-type hydrogen bond found between each HCl_4TPA molecule is generally referred to as a "charge-assisted hydrogen bond", and such types of hydrogen bond tend to be strong and very short [30]. Indeed, the hydrogen bond distance of O5···O5A was 2.458 Å. This value can be recognized as a considerably strong and short hydrogen bond. The two ligands in the Fe(III) complexes were linked to a 1D hydrogen–bonded column through the hydrogen bond between N2 in the ligand and O4 in the carboxyl group. The distance of N2···O4 was 2.892 Å. This value is classified as a weak hydrogen bond. Overall, each hydrogen–bonded column occupied the area surrounded by Fe(III) complexes and extended along the *c*-axis (Figure 2). The dependence of coordination distances around the Fe(III) atom and temperature in **1-Cl** are also listed in Table 1. At 123 K, the distances between Fe1 and N1, N3, and O1 were 1.975(3), 1.925(3), and 1.857(2) Å, respectively. These values indicated that the Fe(III) complex in **1-Cl** at 123 K was in the low-spin (LS) state. Meanwhile, the same coordination distances at 330 K were 2.098(3), 2.112(3), and 1.882(3) Å, respectively. The increment of coordination distances around Fe1 from 123 to 330 K indicates that the Fe(III) complexes in **1-Cl** exhibited SCO from the LS state (S = 1/2) to the high-spin (HS) state (S = 5/2) with increasing temperature. We also determined the crystal structures of **1-Br**, **2-Cl**, and **2-Br** at 123 K. It was confirmed that the crystal structures of **1-Br**, **2-Cl**, and **2-Br** were isostructural to **1-Cl**. The coordination distances around Fe(III) in **1-Br**, **2-Cl**, and **2-Br** at 123 K were characteristic of the LS Fe(III) complex. The hydrogen bond distances between the dicarboxylic acid and Fe(III) complex and between each dicarboxylic acid in **1-Cl**, **1-Br**, **2-Cl**, and **2-Br** were barely different from each other.

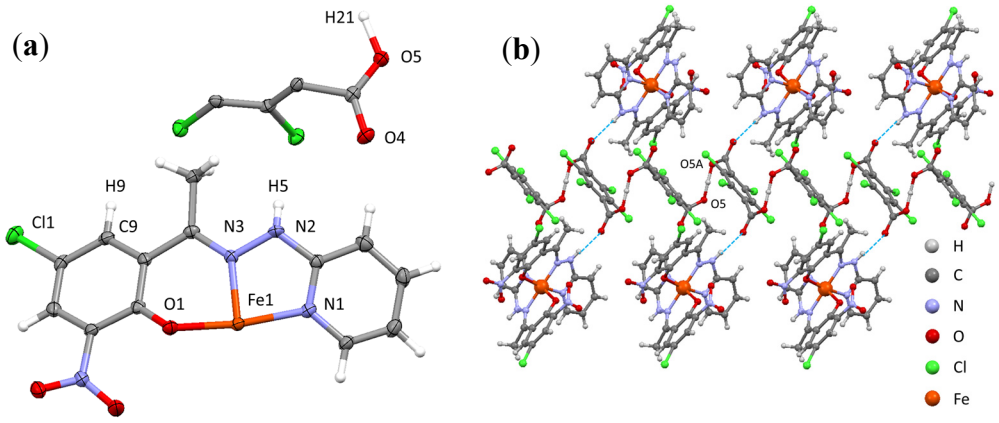

Figure 1. (**a**) Molecular structure of the asymmetric unit; (**b**) Molecular arrangement of the $[Fe(HL1)_2]$ cation and the HCl_4TPA anion. Blue lines represent the hydrogen bonds (N2–H5···O4).

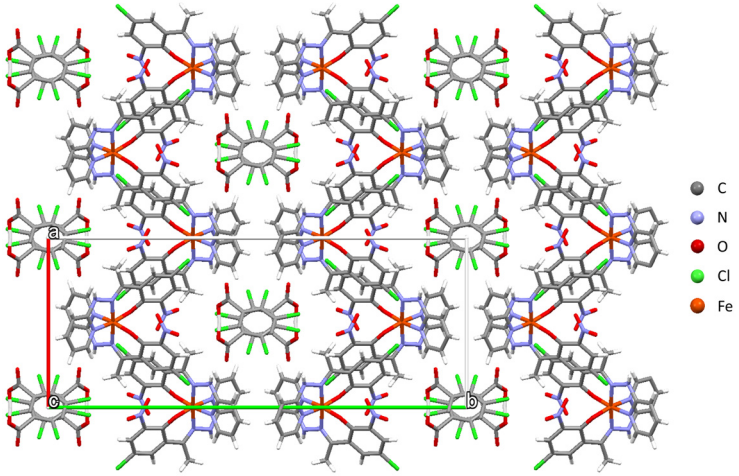

Figure 2. View of the crystal structure of **1-Cl** along the c-axis.

Table 1. Crystallographic data of **1-Cl**, **1-Br**, **2-Cl**, and **2-Br**.

Crystallographic Data					
Compound	**1-Cl**		**1-Br**	**2-Cl**	**2-Br**
Formula	$C_{34}H_{21}Cl_6FeN_8O_{10}$		$C_{34}H_{21}Br_4Cl_2FeN_8O_{10}$	$C_{34}H_{21}Br_2Cl_4FeN_8O_{10}$	$C_{34}H_{21}Br_6FeN_8O_{10}$
Formula weight	970.15		1147.96	1059.05	1236.86
Crystal system	Monoclinic		Monoclinic	Monoclinic	Monoclinic
Space group	*C2/c*		*C2/c*	*C2/c*	*C2/c*
T (K)	123	330	123	123	123
a (Å)	12.479(5)	12.665(3)	12.595(3)	12.627(4)	12.683(7)
b (Å)	30.593(11)	31.287(6)	30.851(7)	30.551(9)	30.984(14)
c (Å)	9.469(3)	9.569(2)	9.607(2)	9.519(3)	9.633(5)
β (°)	96.795(8)	97.326(6)	95.945(5)	96.239(7)	95.330(11)
V (Å^3)	3590(2)	3760.4(13)	3713.2(16)	3650.6(19)	3769.(3)
Z	4	4	4	4	4
D_{cal} (g/cm^3)	1.795	1.713	2.053	1.927	2.179
F (000)	1956.00	1956.00	2244.00	2100.00	2388.00
Data collected	15,405	16,406	16,626	16,224	17,268
Unique data	4069	4272	4242	4197	4309
R(int)	0.0699	0.0783	0.0699	0.0989	0.1157
GOF on F^2	1.115	1.104	1.130	1.106	1.116
R_I [$I > 2\sigma(I)$]	0.0581	0.0659	0.0518	0.0636	0.0579

Table 2. Coordination and hydrogen bond distances in **1-Cl**, **1-Br**, **2-Cl**, and **2-Br**.

Bond lengths Around Fe(III) (Å)					
Compound	**1-Cl**		**1-Br**	**2-Cl**	**2-Br**
Temperature	123 K	330 K	123 K	123 K	123 K
Fe1–N1	1.975(3)	2.098(3)	1.976(4)	1.966(4)	1.980(4)
Fe1–N3	1.925(3)	2.112(3)	1.926(4)	1.923(4)	1.929(4)
Fe1–O1	1.857(2)	1.882(3)	1.857(3)	1.853(3)	1.862(4)
Hydrogen Bond Distances (Å)					
O5···O5A	2.458(3)	2.464(5)	2.463(4)	2.464(5)	2.458(6)
O5–H21	1.233(5)	1.232(7)	1.236(13)	1.235(9)	1.239(12)
N2···O4	2.892(4)	2.890(5)	2.892(5)	2.886(5)	2.872(6)

2.3. Mössbauer Spectroscopy

The variable-temperature Mössbauer spectra of **1-Cl** were measured to identify the spin states and valence of Fe at 123 and 300 K (Figure 3). The spectrum at 123 K shows a single quadrupole doublet. The isomer shift (δ) and quadrupole splitting (ΔE_Q) were 0.179(1) and 2.178(2) mm·s^{-1}, respectively.

The δ and ΔE_Q at 123 K were assigned to the Fe(III) LS isomer. These results were consistent with the prediction from the crystal structure at 123 K. At 300 K, there was a singlet peak without quadrupole splitting. The isomer shift was 0.281(9) mm·s^{-1}, which was assigned to the Fe(III) HS isomer, and this result was also consistent with the spin-state predictions from the crystal structure at 330 K. Overall, the valence of iron in **1-Cl** was confirmed to be Fe(III) (**1-Br**, **2-Cl,** and **2-Br** were isostructural to **1-Cl** and should therefore also be Fe(III)), and the change of coordination distances around Fe with temperature change in the crystal structures originates from the SCO.

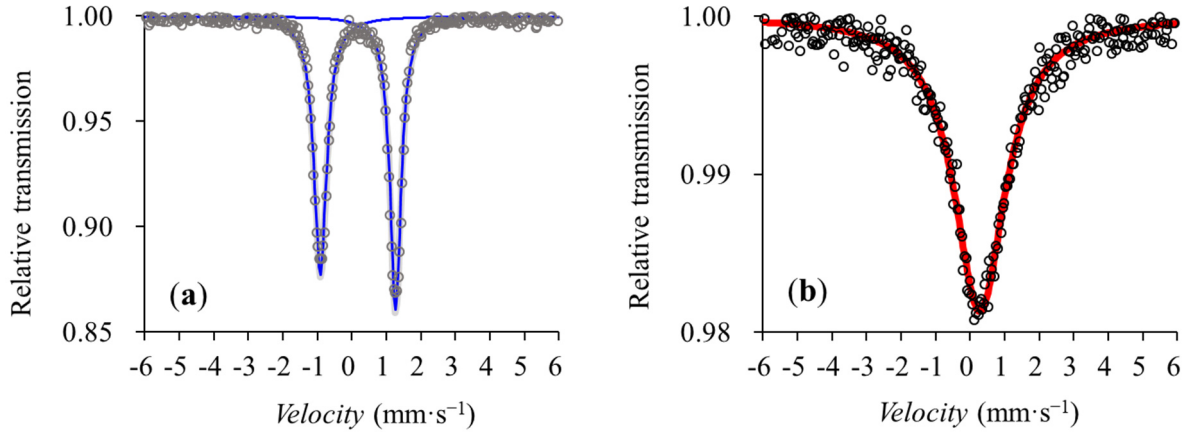

Figure 3. Mössbauer spectra of **1-Cl** at (**a**) 123 K and (**b**) 300 K. Open circles and lines are measurement data and fitting curves, respectively.

2.4. Magnetic Property

The magnetic susceptibility measurements of **1-Cl** and **1-Br** were performed over 100–400 K, whereas those of **2-Cl** and **2-Br** were performed over 150–400 K (Figure 4). At 123 K, the $\chi_m T$ value of **1-Cl** was 0.32 cm^3·K·mol^{-1}, indicating that the Fe(III) complex in **1-Cl**was in the LS state at 123 K. This result is in agreement with the spin-state predictions from the crystal structure and Mössbauer spectra at the same temperature. Additionally, the $\chi_m T$ values of **1-Br**, **2-Cl**, and **2-Br** at 150 K were 0.40, 0.32, and 0.36 cm^3·K·mol^{-1}, respectively; these values also show that **1-Br**, **2-Cl,** and **2-Br** were in the LS state at 150 K. The $\chi_m T$ value of **1-Cl** gradually increased during the heating process as a result of the SCO and ultimately reached 3.72 cm^3·K·mol^{-1} at 400 K. Meanwhile, **1-Br** showed a gradual two-step SCO between 150 and 240 K and finally reached 4.07 cm^3·K·mol^{-1} at 400 K. The spin-transition temperature $T_{1/2}$ in the first and second steps were 188 and 213 K, respectively. However, there was no clear plateau in the two-step SCO in **1-Br**, so the crystal structure of the intermediate phase could not be determined.

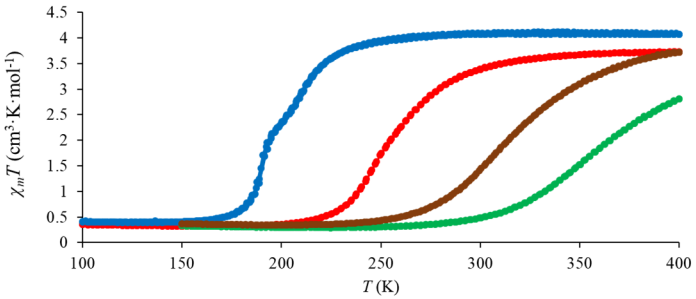

Figure 4. $\chi_m T$–T plots of **1-Br** (blue dots), **1-Cl** (red dots), **2-Br** (brown dots), and **2-Cl** (green dots).

2-Cl and **2-Br** showed gradual SCO near room temperature and finally reached 2.80 and 3.72 cm^3·K·mol^{-1}, respectively. The $\chi_m T$ value for **2-Cl** at 400 K was clearly lower than the expected

value for the HS Fe(III) state (S = 5/2). Additionally, the χT–T plot of **2-Br** still did not reach the plateau region, even at 400 K. For this reason, the SCO of **2-Cl** and **2-Br** were considered incomplete at 400 K. In addition, **2-Cl** and **2-Br** showed a $T_{1/2}$ dependence on the halogen substituent in the dicarboxylic acid, similar to **1-Cl** and **1-Br**. The $\chi_m T$ values of **2-Cl** and **2-Br** in the HT phase were assumed to reach the $\chi_m T$ values of **1-Cl** (3.72 $cm^3 \cdot K \cdot mol^{-1}$) and **1-Br** (4.07 $cm^3 \cdot K \cdot mol^{-1}$) in the HS state, respectively. It was estimated that the $T_{1/2}$ of **2-Cl** and **2-Br** were 373 and 320 K, respectively. The difference of $T_{1/2}$ between **1-Cl** and **1-Br**, or **2-Cl** and **2-Br** clearly showed that the $T_{1/2}$ in SCO complexes coexisting with halogen-substituted dicarboxylic acids can be controlled by changing the halogen substituent in the dicarboxylic acid while keeping the molecular crystal packing. The effect of the halogen substituent change in salicylaldehyde 2-pyridyl hydrazone-type ligands to $T_{1/2}$ was also observed. The $T_{1/2}$ values of **2-Cl** and **2-Br** were clearly shifted to higher temperatures compared with those of **1-Cl** and **1-Br** as the halogen substituent changed from Cl to Br. The shift of $T_{1/2}$ to higher temperatures with the change of halogen substituent in the ligand from Cl to Br was considered to have originated from the electron withdrawing effect of halogen substituents. It is reported that the $T_{1/2}$ of $[Fe(X\text{-}sal_2trien^R)]^+$ that possesses the phonoxide part, which is similar to our ligands, tends to increase with the change of the substituent on the phenoxide part from the OCH_3 substituent possessing electron donor character to the NO_2 possessing electron withdrawing character [31]. It is known that the σ_p Hammett parameter of Br is larger than that of Cl. Thus, the larger electron withdrawing effect of Br compared with that of Cl is considered to induce the shift of $T_{1/2}$ to a higher temperature, which is the same as the case with $[Fe(X\text{-}sal_2trien^R)]^+$.

3. Materials and Methods

3.1. Compound Synthesis

3.1.1. Synthesis of Ligand HL1

The 5′-Chloro-2′-hydroxy-3′-nitroacetophenone (2.2 g; 10 mmol) and 2-hydrazinopyridine (1.1 g; 10 mmol) were dissolved in ethanol (100 mL). The mixture was refluxed for 5 h and left to stand at room temperature. Consequently, yellow needle-shaped crystals were obtained. Anal. $C_{13}H_{11}ClN_4O_3$ (306.05); calcd. C 50.91, H 3.62, N 18.27; found C 50.98, H 3.57, N 18.28.

3.1.2. Synthesis of Ligand HL2

The synthesis procedure for HL2 was identical to that for HL1, except that 5′-bromo-2′-hydroxy-3′-nitroacetophenone was used instead of 5′-chloro-2′-hydroxy-3′-nitroacetophenone. Anal. $C_{13}H_{11}BrN_4O_3$ (350.00); calcd. C 44.46, H 3.16, N 15.96; found C 44.53, H 3.09, N 15.99.

3.1.3. Synthesis of **1-Cl**

H_2L1 (72 mg; 0.20 mmol) was dissolved in methanol (100 mL), and $FeCl_3 \cdot 6H_2O$ (27 mg; 0.10 mmol) was added to the solution. The mixture was stirred for 30 min. Subsequently, H_2Cl_4TPA (30 mg; 0.10 mmol) was added, and the mixture was stirred for 30 s. Then, trimethylamine (14 µL; 0.10 mmol) was added to the solution. The solution was left to stand for several days. Consequently, plate-shaped crystals were obtained. Anal. $C_{34}H_{21}Cl_6FeN_8O_{10}$ (970.13); calcd. C 42.09, H 2.18, N 11.55; found C 42.18, H 2.22, N 11.52.

3.1.4. Synthesis of **1-Br**

The synthesis procedure for **1-Br** was identical to that for **1-Cl**, except that H_2Br_4TPA was used instead of H_2Cl_4TPA. Plate-shaped crystals were obtained. Anal. $C_{34}H_{21}Cl_2Br_4FeN_8O_{10}$ (1147.95); calcd. C 35.57, H 1.84, N 9.76; found C 35.69, H 1.88, N 9.79.

3.1.5. Synthesis of **2-Cl**

The synthesis procedure for **2-Cl** was identical to that for **1-Cl**, except that H_2L2 was used instead of H_2L1. Plate-shaped crystals were obtained. Anal. $C_{34}H_{21}Cl_4Br_2FeN_8O_{10}$ (1059.04); calcd. C 38.56, H 2.00, N 10.58; found C 38.53, H 2.04, N 10.51.

3.1.6. Synthesis of **2-Br**

The synthesis procedure for **2-Br** was identical to that for **1-Br**, except that HL2 was used instead of HL1. Plate-shaped crystals were obtained. Anal. $C_{34}H_{21}Br_6FeN_8O_{10}$ (1236.86); calcd. C 33.02, H 1.71, N 9.06; found C 33.02, H 1.73, N 9.01.

3.2. X-ray Structure Determination

Diffraction data from **1-Cl** at 123 and 330 K and **1-Br**, **2-Cl**, and **2-Br** at 123 K were collected on a Rigaku charge-coupled device diffractometer (Rigaku, Tokyo, Japan). A crystal was glued onto a nylon loop and enveloped in a temperature-controlled stream of dry N_2 gas during data collection. The structures were solved by direct methods and refined with full-matrix least-squares procedures using the *SHELXS-97* program. Hydrogen atoms involved in the hydrogen bonds were determined from the Fourier difference map, and other hydrogen atoms were generated by calculations and refined using a riding model. All non-hydrogen atoms were refined anisotropically. CCDC 1543784 (**1-Cl 123 K**), 1543783 (**1-Cl 330 K**), 1543785 (**1-Br 123 K**), 1543786 (**2-Cl 123 K**), and 1543787 (**2-Br 320 K**) contain the supplementary crystallographic data for this paper. These data can be obtained free of charge via http://www.ccdc.cam.ac.uk/conts/retrieving.html or from the CCDC (12 Union Road, Cambridge CB2 1EZ, UK; Fax: +44-1223-336033; E-mail: deposit@ccdc.cam.ac.uk).

3.3. ^{57}Fe Mössbauer Spectroscopy

^{57}Fe Mössbauer spectra were recorded using a CryoMini/CryoStat cryogenic refrigerator set (Iwatani Industrial Gases, Osaka, Japan) and a conventional Mössbauer spectrometer (Topologic Systems, Kanagawa, Japan) with a ^{57}Co/Rh source. The spectra were calibrated by using the six lines of a body-centered cubic iron foil (α-Fe), the center of which was taken as the zero isomer shift. The Mössbauer spectra were fitted with the least-squares fitting program MossWinn 4.0 [32].

3.4. Magnetic Property Measurements

Magnetic measurements were performed on a Quantum Design MPMS-5S superconducting quantum-interference device magnetometer (Quantum Design, Inc., San Diego, CA, USA), and data were corrected for the diamagnetic contribution, as calculated from Pascal's constants. Temperature sweeping mode was used to collect the data at a sweep rate of 1 K·min^{-1} with a magnetic field of 5 kOe.

4. Conclusions

In brief, we synthesized four Fe(III) SCO compounds that contained a halogen-substituted salicylaldehyde 2-pyridyl hydrazone-type ligand complex with a dicarboxylic acid as the anion. Crystal structures confirmed that all the compounds were isostructural. Furthermore, the dicarboxylic acid anion formed a 1D hydrogen–bonded column, and the Fe(III) complex formed weak hydrogen bonds with the 1D hydrogen–bonded column. Mössbauer spectroscopy for **1-Cl** demonstrated that the valence of the iron center was Fe(III), and these compounds showed SCO. The magnetic property measurements of these compounds showed that they exhibited gradual SCO, and the spin-transition temperature shifted to higher values without changing the molecular crystal packing when the halogen substituent in the dicarboxylic acid changed from Br to Cl. Additionally, it was confirmed that the change of halogen substituent in the salicylaldehyde 2-pyridyl hydrazone-type ligands from Cl to Br shifts $T_{1/2}$ to a higher temperature while still maintaining the molecular crystal packing. The shift of

$T_{1/2}$ when a halogen substituent is changed within the in the ligand is considered to have originated from the difference in the electron-withdrawing effect of Cl and Br. In conclusion, the spin-transition temperature of Fe(III) complexes bearing salicylaldehyde 2-pyridyl hydrazone-type ligands can be adjusted by introducing a halogen-substituted dicarboxylic acid and changing the halogen substituent in the dicarboxylic acid or the ligand.

Supplementary Materials: The following are available online at www.mdpi.com/2304-6740/5/3/53/s1. Cif and cif-checked files.

Author Contributions: Takumi Nakanishi and Osamu Sato designed the compounds and measured the magnetic properties and crystal structures. Atsushi Okazawa operated the ^{57}Fe Mössbauer spectrometer and analyzed the Mössbauer spectra.

Conflicts of Interest: The authors declare no conflicts of interest.

References

1. Gülich, P.; Hauser, A. Thermal and light-induced spin crossover in iron(II) complexes. *Coord. Chem. Rev.* **1990**, *97*, 1–22. [CrossRef]
2. Sato, O. Optically switchable molecular solids: Photoinduced spin-crossover, photochromism, and photoinduced magnetization. *Acc. Chem. Res.* **2003**, *36*, 692–700. [CrossRef] [PubMed]
3. Real, J.A.; Gaspar, A.B.; Munoz, M.C. Thermal, pressure and light switchable spin-crossover materials. *Dalton Trans.* **2005**, 2062–2079. [CrossRef] [PubMed]
4. Kershaw Cook, L.J.; Kulmaczewski, R.; Mohammed, R.; Dudley, S.; Barrett, S.A.; Little, M.A.; Deeth, R.J.; Halcrow, M.A. A unified treatment of the relationship between ligand substituents and spin state in a family of iron(II) complexes. *Angew. Chem. Int. Ed.* **2016**, *55*, 4327–4331. [CrossRef] [PubMed]
5. Halcrow, M.A. The effect of ligand design on metal ion spin state-lessons from spin crossover complexes. *Crystals* **2016**, *6*, 20. [CrossRef]
6. Sato, O. Dynamic molecular crystals with switchable physical properties. *Nat. Chem.* **2016**, *8*, 644–656. [CrossRef] [PubMed]
7. Lemercier, G.; Brefuel, N.; Shova, S.; Wolny, J.A.; Dahan, F.; Verelst, M.; Paulsen, H.; Trautwein, A.X.; Tuchagues, J.P. A range of spin-crossover temperature $T_{1/2} > 300$ k results from out-of-sphere anion exchange in a series of ferrous materials based on the 4-(4-imidazolylmethyl)-2-(2-imidazolylmethyl)imidazole (trim) ligand, $[Fe(trim)_2]X_2$ (X=F, Cl, Br, I): Comparison of experimental results with those derived from density functional theory calculations. *Chem. Eur. J.* **2006**, *12*, 7421–7432. [PubMed]
8. Paulsen, H.; Duelund, L.; Zimmermann, A.; Averseng, F.; Gerdan, M.; Winkler, H.; Toftlund, H.; Trautwein, A.X. Substituent effects on the spin-transition temperature in complexes with tris(pyrazolyl) ligands. *Mon. Chem.* **2003**, *134*, 295–306. [CrossRef]
9. Wei, R.-J.; Tao, J.; Huang, R.-B.; Zheng, L.-S. Anion-dependent spin crossover and coordination assembly based on $[Fe(tpa)]^{2+}$[tpa = tris(2-pyridylmethyl)amine] and $[N(CN)_2]^-$: Square, zigzag, dimeric, and [4 + 1]-cocrystallized complexes. *Eur. J. Inorg. Chem.* **2013**, *2013*, 916–926. [CrossRef]
10. Zhang, W.; Zhao, F.; Liu, T.; Yuan, M.; Wang, Z.M.; Gao, S. Spin crossover in a series of iron(II) complexes of 2-(2-Alkyl-2*H*-tetrazol-5-yl)-1,10-phenanthroline: Effects of alkyl side chain, solvent, and anion. *Inorg. Chem.* **2007**, *46*, 2541–2555. [CrossRef] [PubMed]
11. Zhu, Y.Y.; Li, H.Q.; Ding, Z.Y.; Lu, X.J.; Zhao, L.; Meng, Y.S.; Liu, T.; Gao, S. Spin transitions in a series of $[Fe(pybox)_2]^{2+}$ complexes modulated by ligand structures, counter anions, and solvents. *Inorg. Chem. Front.* **2016**, *3*, 1624–1636. [CrossRef]
12. Ivanova, T.A.; Ovchinnikov, I.V.; Turanov, A.N. Influence of the outersphere anion on the properties of the spin transition in Fe(4-OCH3-SalEen)$_2$ Y (Y = PF_6, NO_3). *Phys. Solid State* **2007**, *49*, 2132–2137. [CrossRef]
13. Nemec, I.; Herchel, R.; Travnicek, Z. The relationship between the strength of hydrogen bonding and spin crossover behaviour in a series of iron(III) Schiff base complexes. *Dalton Trans.* **2015**, *44*, 4474–4484. [CrossRef] [PubMed]
14. Phonsri, W.; Harding, D.J.; Harding, P.; Murray, K.S.; Moubaraki, B.; Gass, I.A.; Cashion, J.D.; Jameson, G.N.; Adams, H. Stepped spin crossover in Fe(III) halogen substituted quinolylsalicylaldimine complexes. *Dalton Trans.* **2014**, *43*, 17509–17518. [CrossRef] [PubMed]

15. Phonsri, W.; Macedo, D.S.; Vignesh, K.R.; Rajaraman, G.; Davies, C.G.; Jameson, G.N.L.; Moubaraki, B.; Ward, J.S.; Kruger, P.E.; Chastanet, G.; et al. Halogen substitution effects on N2O Schiff base ligands in unprecedented abrupt Fe^{II} spin crossover complexes. *Chem. Eur. J.* **2017**, *23*, 7052–7065. [CrossRef] [PubMed]
16. Ueno, T.; Miyano, K.; Hamada, D.; Ono, H.; Fujinami, T.; Matsumoto, N.; Sunatsuki, Y. Abrupt spin transition and chiral hydrogen-bonded one-dimensional structure of iron(III) complex $[Fe^{III}(Him)_2(hapen)]SbF_6$ (Him = imidazole, H_2hapen = *N*,*N*′-bis(2-hydroxyacetophenylidene)ethylenediamine). *Magnetochemistry* **2015**, *1*, 72. [CrossRef]
17. Nakanishi, T.; Sato, O. Synthesis, structure, and magnetic properties of new spin crossover Fe(II) complexes forming short hydrogen bonds with substituted dicarboxylic acids. *Crystals* **2016**, *6*, 8. [CrossRef]
18. Koningsbruggen, P.J.; Maeda, Y.; Oshio, H. Iron(III) spin crossover compounds. *Spin Crossover Transit. Metal Compd. I* **2004**, *233*, 259–324.
19. Nihei, M.; Shiga, T.; Maeda, Y.; Oshio, H. Spin crossover iron(III) complexes. *Coord. Chem. Rev.* **2007**, *251*, 2606–2621. [CrossRef]
20. Hayami, S.; Gu, Z.; Yoshiki, H.; Fujishima, A.; Sato, O. Iron(III) spin-crossover compounds with a wide apparent thermal hysteresis around room temperature. *J. Am. Chem. Soc.* **2001**, *123*, 11644–11650. [CrossRef] [PubMed]
21. Li, Z.Y.; Dai, J.W.; Shiota, Y.; Yoshizawa, K.; Kanegawa, S.; Sato, O. Multi-step spin crossover accompanied by symmetry breaking in an Fe(III) complex: Crystallographic evidence and DFT studies. *Chem. Eur. J.* **2013**, *19*, 12948–12952. [CrossRef] [PubMed]
22. Phonsri, W.; Davies, C.G.; Jameson, G.N.; Moubaraki, B.; Murray, K.S. Spin crossover, polymorphism and porosity to liquid solvent in heteroleptic iron(III) {quinolylsalicylaldimine/thiosemicarbazone-salicylaldimine} complexes. *Chem. Eur. J.* **2016**, *22*, 1322–1333. [CrossRef] [PubMed]
23. Fujinami, T.; Ikeda, M.; Koike, M.; Matsumoto, N.; Oishi, T.; Sunatsuki, Y. Syntheses, hydrogen-bonded assembly structures, and spin crossover properties of $[Fe^{III}(Him)_2$(n-MeOhapen)]PF_6 (Him = imidazole and n-MeOhapen = *N*,*N*′-bis(n-methoxy-2-oxyacetophenylidene)ethylenediamine); n = 4, 5, 6). *Inorg. Chim. Acta* **2015**, *432*, 89–95. [CrossRef]
24. Tang, J.; Sanchez Costa, J.; Smulders, S.; Molnar, G.; Bousseksou, A.; Teat, S.J.; Li, Y.; van Albada, G.A.; Gamez, P.; Reedijk, J. Two-step spin-transition iron(III) compound with a wide [high spin-low spin] plateau. *Inorg. Chem.* **2009**, *48*, 2128–2135. [CrossRef] [PubMed]
25. Anderson, R.G.; Nickless, G. Co-ordinating properties of some ligand systems related to 4-(2-pyridylazo)resorcinol. *Talanta* **1967**, *14*, 1221–1228. [CrossRef]
26. Basu, C.; Chowdhury, S.; Banerjee, R.; Evans, H.S.; Mukherjee, S. A novel blue luminescent high-spin iron(III) complex with interlayer O–HCl bridging: Synthesis, structure and spectroscopic studies. *Polyhedron* **2007**, *26*, 3617–3624. [CrossRef]
27. Liu, H.Y.; Gao, F.; Niu, D.Z. Synthesis and structure of iron(III) complex with N,N,O-donor aroylhydrazones: The chloride anion as hydrogen bond acceptor forming infinite chains. *Asian J. Chem.* **2011**, *23*, 2014–2016.
28. Zhang, J.; Campolo, D.; Dumur, F.; Xiao, P.; Fouassier, J.P.; Gigmes, D.; Lalevee, J. Iron complexes as photoinitiators for radical and cationic polymerization through photoredox catalysis processes. *J. Polym. Sci. Pol. Chem.* **2015**, *53*, 42–49. [CrossRef]
29. Mohan, M.; Gupta, N.S.; Chandra, L.; Jha, N.K. Synthesis, characterization and antitumor properties of some metal–complexes of 3-substituted and 5-substituted salicylaldehyde 2-pyridinylhydrazones. *J. Inorg. Biochem.* **1987**, *31*, 7–27. [CrossRef]
30. Dega-Szafran, Z.; Katrusiak, A.; Szafran, M. Short and symmetrical OHO hydrogen bond in bis(quinuclidine betaine) hydrochloride. *J. Mol. Struct.* **2010**, *971*, 1–7. [CrossRef]
31. Tweedle, M.F.; Wilson, L.J. Variable spin iron(III) chelates with hexadentate ligands derived from triethylenetetramine and various salicylaldehydes—Synthesis, characterization, and solution state studies of a new ^{2}T reversible ^{6}A spin equilibrium system. *J. Am. Chem. Soc.* **1976**, *98*, 4824–4834. [CrossRef]
32. Klencsár, Z. MossWinn Manual. 2016. Available online: http://www.mosswinn.hu/downloads/mosswinn.pdf (accessed on 26 April 2017).